

Supporting Information

Highly Stretchable and Autonomously Healable Epidermal Sensor Based on Multi-Functional Hydrogel Frameworks

Gang Ge,^a Wei Yuan,^a Wen Zhao,^a Yao Lu,^a Yizhou Zhang,^a Wenjun Wang,^b Peng Chen,^c

Wei Huang,^{ad} Weili Si^{*a} and Xiaochen Dong^{*a}

^aKey Laboratory of Flexible Electronics (KLOFE) & Institute of Advanced Materials (IAM),

Nanjing Tech University (NanjingTech), 30 South Puzhu Road, Nanjing 211800, China.

E-mail: iamxcdong@njtech.edu.cn; iamwlsi@njtech.edu.cn

^bSchool of Physical Science and Information Technology, Liaocheng University, Liaocheng

252059, China

^cSchool of Chemical and Biomedical Engineering, Innovative Centre for Flexible Devices,

Nanyang Technological University, 62 Nanyang Drive, 637459, Singapore

^dShaanxi Institute of Flexible Electronics (SIFE), Northwestern Polytechnical University

(NPU), 127 West Youyi Road, Xi'an 710072, China

Supporting Information

Experimental Section

Materials: Ammonium persulfate (APS), iron nitrate nonahydrate, sodium dodecyl sulfate (SDS), multi-walled carbon nanotube (MWCNT) and ethylene glycol (EG) were purchased from Sigma-Aldrich. Acrylic acid (AA, 98%), N, N-methylenebisacrylamide (MBAA), N,N,N',N'-tetramethylethylenediamine (TEMED), N,N-dimethylformamide (DMF), polyvinyl pyrrolidone (PVP), poly(3,4-ethylenedioxythiophene):polystyrene sulfonate (PEDOT:PSS) were purchased from Adamas-beta. Borax and polyvinyl alcohol (PVA) were purchased from Tansoole (Shanghai). In this work, all chemicals were directly used for hydrogel synthesis without further purification.

Functionalized Multi-Walled Carbon Nanotube (F-MWCNT): The functionalization of MWCNT was conducted according to a reported procedure with modification.¹ Briefly, 5 mg of SDS was dissolved in deionized water under stirring for 10 min. Then MWCNT was added to the above solution and exposed to ultrasonication (SCIENTZ, JY-88IIN) for another 45 min at room temperature. Thereafter, the obtained slurry was placed in a centrifuge tube and centrifuged at 11000 rpm. After 10 min, the supernate was carefully collected in a beaker, to which several milligrams of PVP was added, followed by ultrasonication and centrifugation. To increase the dispersibility of MWCNT, DMF and DI water were added to the as-mentioned solution. Clear and uniform F-MWCNT suspension was obtained after all the procedures.

Synthesis of Binary Networked Hydrogel: A one-step approach was utilized to synthesize binary-networked hydrogel. In detail, 0.151 mmol iron nitrate nonahydrate was dissolved in 6 mL deionized water (DI water) under stirring. After dissolving MBAA and borax powder

Supporting Information

in the as-mentioned solution, 0.164 mmol APS was added. Afterwards, 2 mL EG and 3 mL PVA solution (9 wt%) were added to the precursor solution. To increase the mechanical and piezoresistive performance of the hydrogel, the as-prepared soluble MWCNT slurry and PEDOT:PSS were added. The final concentration of modified F-MWCNT in precursor solution was 2 mg/mL. Subsequently, 10 μ L TEMED and an appropriate amount of AA monomer were added dropwise to the above precursor. MBAA and TEMED were chemical crosslinker and accelerator for the formation of polyacrylic acid networks respectively.

Before preparing free-standing hydrogels, the precursor was well mixed under magnetic stirring and ultrasonication to obtain homogeneous solution. After that, the homogeneous precursor was degassed for 10 min with N₂ gas to remove air bubbles. Afterwards, the hydrogel precursor solution was poured into a petri dish ($\Phi = 55$ mm) mold under room temperature to prepare self-healing and anti-freezing hydrogels. After 2 hours, the monolithic hydrogel was rinsed by adequate DI water to eliminate excessive EG and superfluous ions. Finally, hair drier was used to blow away residual DI water and enhance the mechanical-compliance performance of the self-healing hydrogel. A larger petri dish ($\Phi = 90$ mm) was utilized for large scale preparation of the self-healing hydrogel film with the other conditions being the same as described above.

Mechanical performance Tests: All the mechanical tests were conducted on a customized tensile-compressive tester Mark-10, which incorporated both computer-controlled test platforms and stretching clamps. For the compressive tests, a cylindrical hydrogel (45 mm in diameter and 5 mm in thickness) was placed on the planar platform. For cyclic compression-recovery measurement, the deformation speed was set as 40 mm/min. For the tensile tests, a

Supporting Information

rectangular hydrogel piece (10 mm in length, 2 mm in thickness and 8 mm in width) was clamped between two clamps and the stretching speed was fixed at 40 mm/min. Note that the nominal stress (δ) is calculated by the following formula:

$$\delta = F/A$$

where F is the stretching load and A is the cross-sectional areas. Elastic modulus (E) is achieved from the linear region of stress-strain curve. Strain (ε) is estimated by the formula:

$$\varepsilon = \Delta L/L_0 \times 100 \%$$

Where L_0 is the initial length of the specimen without stretching, $\Delta L (= L - L_0)$ is the length change under stretching condition.

Evaluation of the Mechanical Self-Healing Efficiency of the Hydrogel: The as-prepared monolithic hydrogel film was cut into strip-shaped samples and stretched to its breakage point, in which process the tensile curve versus time was synchronously recorded. For recovery of the mechanical property, the cracked specimen was brought into contact instantly under ambient condition. To accelerate the self-healing process, heat was necessary to boost the mechanical recovery rate. After self-healing for different hours (2, 4 and 6 hours), the healed hydrogel films were stretched to a second breakage and the stress-strain curves were recorded by the mechanical testing platform respectively. For different self-healing times (the 1st, 2nd and 3rd self-healing process) characterization, the healed samples were stretched to rupture again. Such processes were repeated for three times. The stress and strain of healed samples were evaluated from the formula mentioned above. The mechanical healing efficiency (f_M) was defined by the formula below:

$$f_M = \varepsilon'/\varepsilon \times 100\%$$

Supporting Information

where ε' is the strain of the sample with scratched scar (broken hydrogel film after self-healing), ε is the strain of the integral sample (original hydrogel film).

Hydrogel Based Flexible Sensor Fabrication: The free-standing conductive hydrogel film was cut into a strip-shaped specimen. Note that the residue and superfluous water on the hydrogel surface were blown away by a hair drier to obtain stable electrical output. Afterwards, conductive copper sheets were tightly adhered on the opposite covers of the hydrogel by semi-transparent adhesive tapes to assemble into a sandwich-like flexible sensor. The intrinsic toughness of the self-healing conductive hydrogel was beneficial for device assembly. Adhesive medical tapes were utilized to encapsulate the device to avoid electric leakage and minimize ambient interference on the piezoresistive performances of the flexible sensor.

Strain- and Pressure-Sensing Measurements: To obtain the piezoresistive behavior of flexible sensor under external pressure, various pressures were applied on the sensor, and the deformation speed was set as 20 mm/min. For response time and cyclic durability characterization, the pressure deformation speed was set as 330 mm/min. For stretchable sensor assembly, both sides of the conductive hydrogel were encapsulated by adhesive tapes, which were clamped by the stretchable clip of computer-controlled Mark-10. The stretching speed was set as 40 mm/min and the instant electrical output signals upon stretching were recorded by Keithley 4200-SCS. Care should be taken that no puncture was applied on the hydrogel due to its pulpy state.

Evaluation of the Electrical Self-Healing Efficiency of the Hydrogel: The flexible sensor based on hydrogel film was utilized to assess the piezoresistive property. After stable

Supporting Information

electrical signal was obtained, the monolithic hydrogel was cut into two pieces by a razor blade to separate both parts completely. Note that the electrical self-healing performance of the hydrogel requires no external stimulus, such as heat, UV light and additional chemicals. The two separated segments left under ambient condition can recover to its original electrical state. The current value of the sample was simultaneously recorded by a semiconductor characterization system.

Anti-Freezing Characterization of Conductive Hydrogel Film: The hydrogel was prepared by the as-mentioned procedure. After rinsing in deionized water, the hydrogel was cut into strip-shaped film (10 mm in length, 2 mm in thickness and 8 mm in width) and placed in a refrigerator under -25 °C for 12 hours. After thorough freezing, the hydrogel film was taken out and the ice on the hydrogel film surface was removed. The ice was from water within the hydrogel and the ambient environment. The tensile mechanical test was instantly conducted after the thawing process.

Synthesis of PAA-Based Unitary Networked Self-Healing Hydrogel: Unitary Networked PAA-based self-healing hydrogel was prepared following by the same procedure without addition of PVA and borax powder. After stretching to the breakage point, two pieces of the PAA-based self-healing hydrogel was brought into contact instantly. Mechanical tests were conducted after certain healing time and the stress-strain curves were simultaneously recorded.

Synthesis of PVA-Based Unitary Networked Self-Healing Hydrogel: 3 mL PVA solution (9 wt%) was poured into a beaker, followed by addition of DMF, F-MWCNT and EG. All the chemicals were sonicated for 30 min to prepare uniform solution A. Borax and 0.5 mL

Supporting Information

PEDOT:PSS dissolved in 3 mL DI water were added into another beaker, marked as solution B. Before preparing hydrogel, solution A and B were subjected to vacuum drying to eliminate bubbles. Thereafter, solution A and B were mixed quickly to form hydrogel. Note that the hydrogel was left under ambient environment to enhance the mechanical strength.

Supporting Information

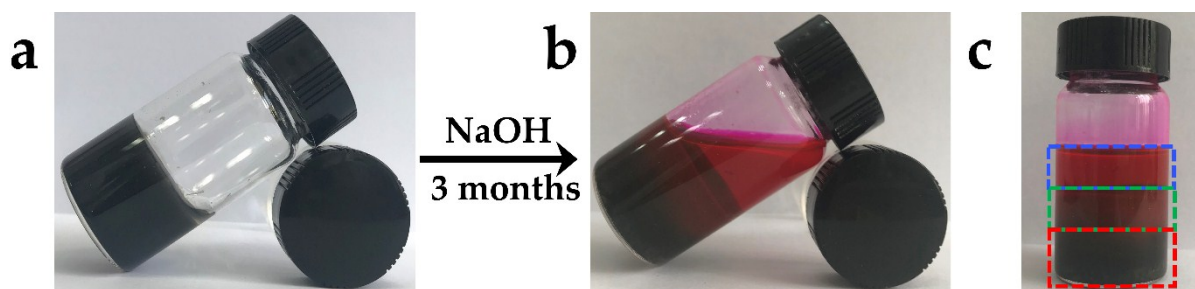


Figure S1. (a) The pristine hydrogel. (b) Monolithic sample immersed by sodium hydroxide solution for three months. The solution was stained by rhodamine B to give a clear distinction. (c) The state of the sample after three months. It is noted that the system incorporates three parts: homogeneous solution, buffer layer and hydrogel bulk. PAA-based hydrogel behaved high swelling ratio in sodium hydroxide due to the breakage of intermolecular bonds.²

Supporting Information

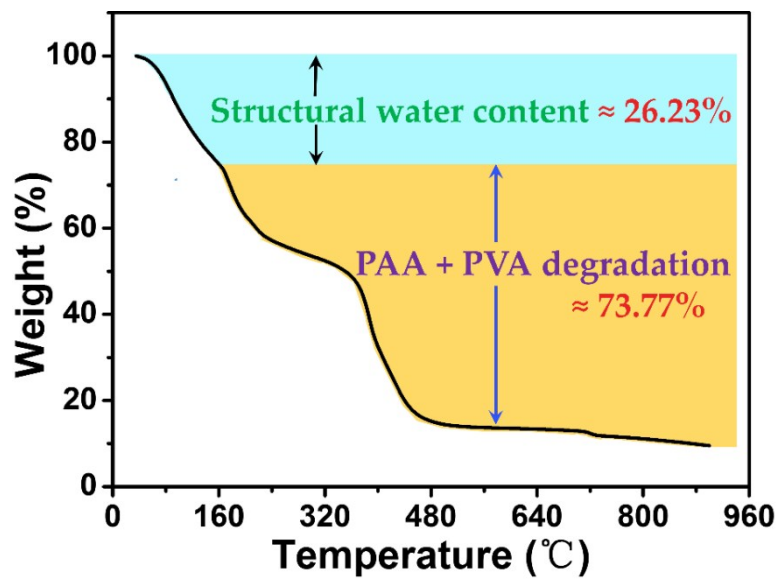


Figure S2. Thermal gravimetric analysis (TGA) of the dried hydrogel sample.

Supporting Information

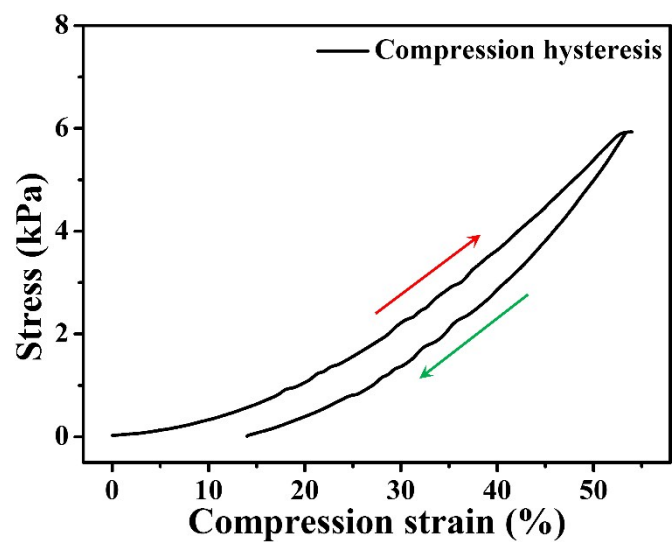


Figure S3. Hysteresis performance of the sample during compression process. The hysteresis was evaluated according to the maximal difference between the loading and unloading curve.³

Supporting Information



Figure S4. Photograph of the highly adhesive hydrogel attached to human epidermis.

Supporting Information

Table S1. Comparison of reported hydrogels with this work.

References	Materials	Interactive Types	Maximal Strain (%)
4	Ca ²⁺ /glycerol/ silk fibroin protein/Ag NWs	chelation/charge interaction	400
5	β-cyclodextrin/adamantanebased monomers	dynamic host-guest interactions/crack bridging	50
6	PVA	hydrogen bonding	400
7	GelMA/TA	hydrogen bonding interaction/plasticization effect	250
8	PDMS/benzophenone/ polyacrylamide	chemical crosslinking/ chemical anchoring	330
9	PVA/PDA/sodium tetraborate	reversible boron ester bonding	400
10	Ca ²⁺ /Fe ³⁺ /alginate/ polyacrylamide	ionic crosslinking/ covalent crosslinking	375
11	F-PNIPAAm/PANI	topological crosslinking/ chemical crosslinking	290
12	PANI/GO	intermolecular interaction	40
13	PVA/PANI/boronic acid/ABA	covalent crosslinking/ intermolecular interaction	250
14	PCL-PEG-PCL	hydrophobic interactions/chemical crosslinking	180
15	PAA-co-DMAPS	hydrogen bonding/ionic associations/hydration effect/ hydrophobic interactions	100
16	gelatin/(NH ₄) ₂ SO ₄	Hofmeister effect/hydrophobic interactions	500
17	Ppy/agarose	hydrogen bonding	40
18	PEG/alginate/Ca ²⁺ / nanoclay	covalent crosslinking/ionic crosslinking	500
This work	PAA/PVA/Fe ³⁺ / borax/CNT/EG	chemical crosslinking/ ionic crosslinking/ hydrogen bonding	550

Supporting Information

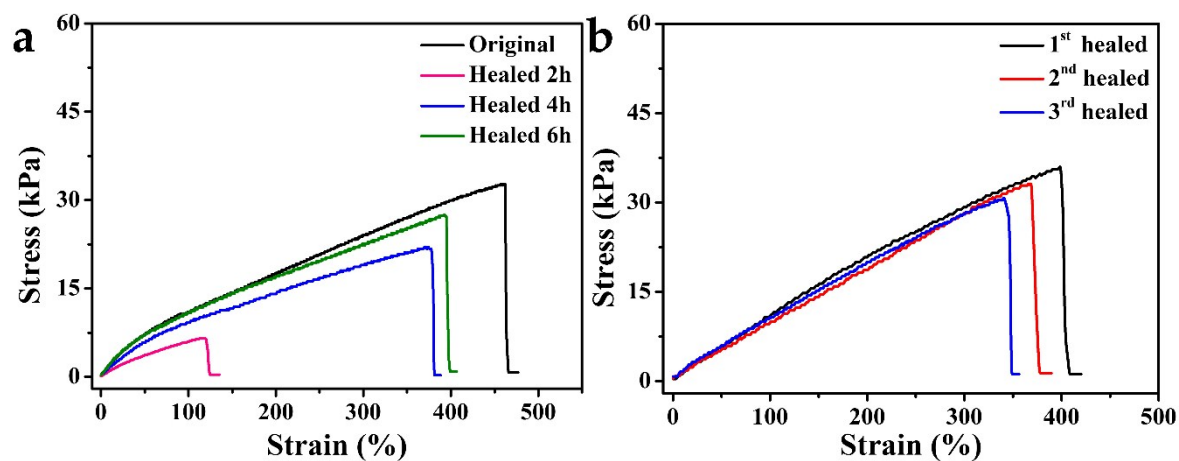


Figure S5. The stress-strain curves of unitary PAA-networked hydrogel after different healing (a) hours and (b) durations. Note that the unitary PAA-networked hydrogel behaves high healed strain within shorter healing time compared with reported literatures.¹⁹

Supporting Information

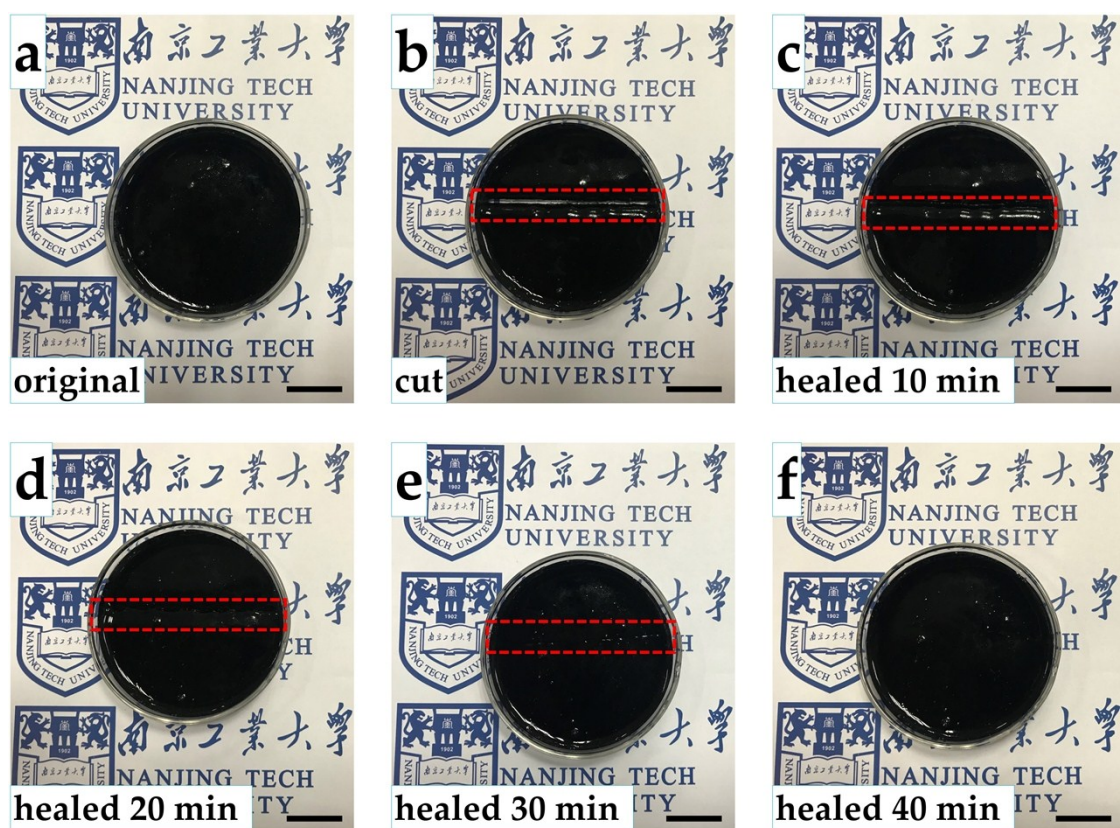


Figure S6. Photographs of unitary PVA-networked hydrogel after different healing time.

High healing efficiency is presented, which is advantageous to literatures.^{20, 21} Scale bar: 3

cm.

Supporting Information

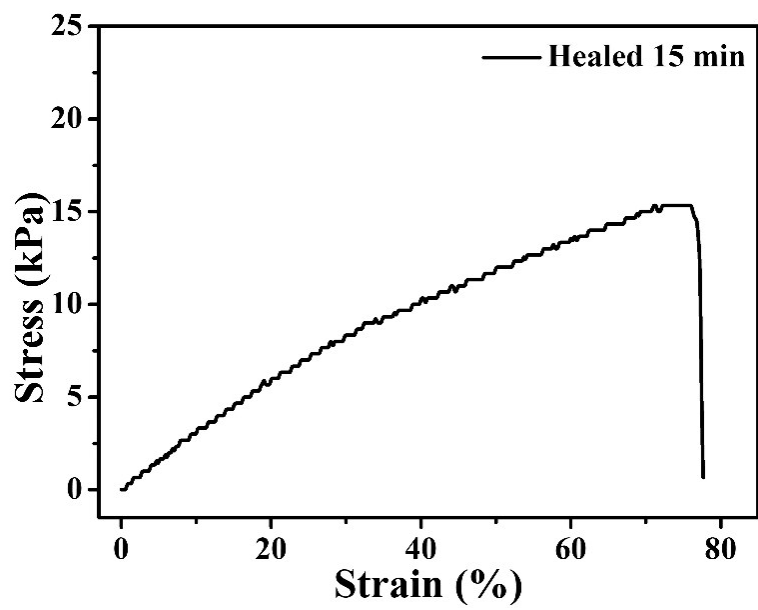


Figure S7. Fast healing process of the hydrogel.

Supporting Information

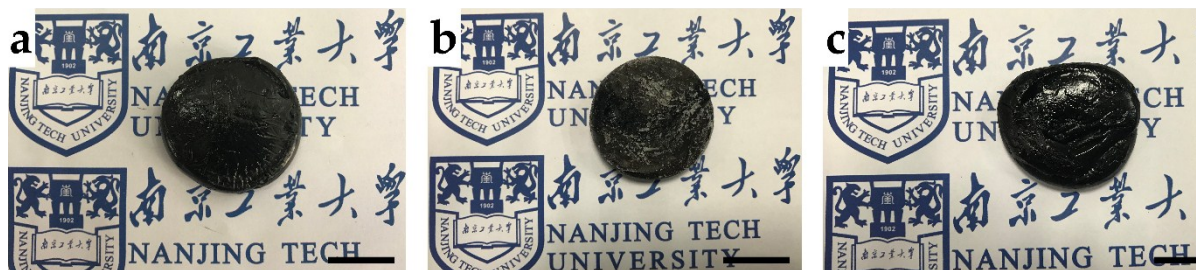


Figure S8. Anti-freezing performance of the hydrogel. (a) The original hydrogel. (b) Hydrogel treated under subzero temperature. (c) Hydrogel recovered under room temperature.

Supporting Information

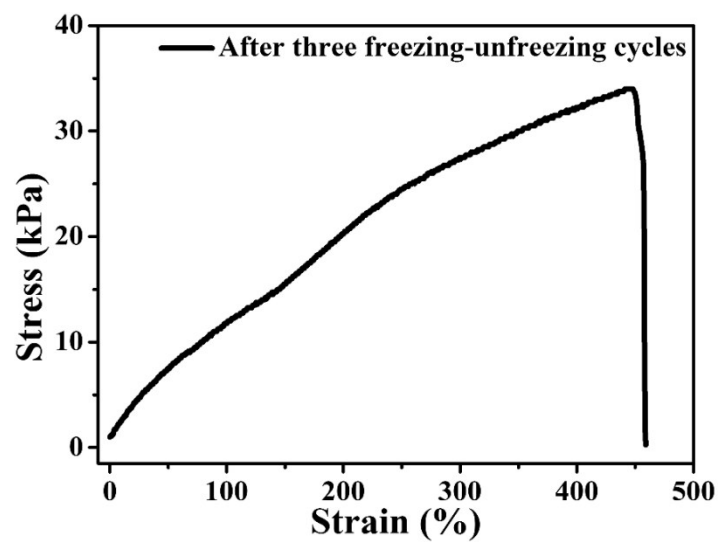


Figure S9. The stress-strain curve of the hydrogel after three freezing-thawing cycles.

Supporting Information

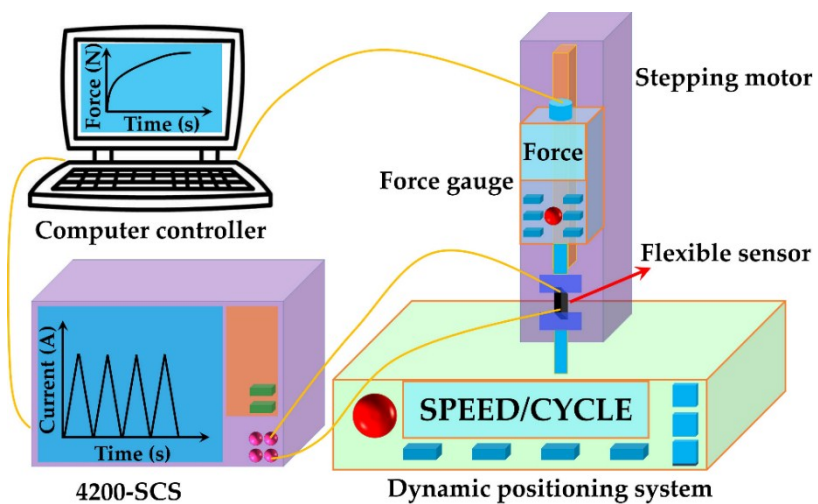


Figure S10. The schematic illustration of the experimental setup for the measurement of flexible sensor.

Supporting Information

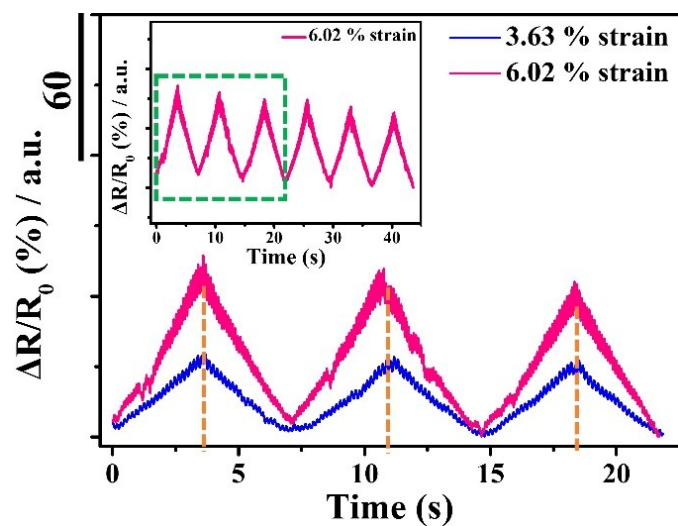


Figure S11. Relative resistance variation upon different strains (3.63% and 6.02%). The top left image shows electrical output upon durable dynamic deformation.

Supporting Information

Table S2. Sensing performances of our sensor and other references.

References	Applications	Workable Ranges (kPa/%)		S (kPa ⁻¹)/GF	
22	Strain sensor	0-40%	40-60%	0.23	0.76
23	Pressure sensor	0-10k Pa	10-50 kPa	8.6 kPa ⁻¹	50 kPa ⁻¹
24	Pressure sensor	0-350 kPa	-	0.023 kPa ⁻¹	-
25	Pressure sensor	0-0.4 kPa	0.4-2 kPa	0.149 kPa ⁻¹	0.015 kPa ⁻¹
26	Pressure sensor	0-6 kPa	6-10 kPa	0.05 kPa ⁻¹	0.01 kPa ⁻¹
27	Pressure sensor	0-1 kPa	-	0.17 kPa ⁻¹	-
28	Strain sensor	0-100%	100-1000%	0.24	1.51
29	Strain sensor	0-200%	-	0.478	-
30	Pressure sensor	0-1.2 kPa	1.2-1.8 kPa	9.32 kPa ⁻¹	5.09 kPa ⁻¹
31	Pressure sensor	0-3 kPa	3-6 kPa	0.041 kPa ⁻¹	0.24 kPa ⁻¹
32	Pressure sensor	0-1 kP	-	0.09 kPa ⁻¹	-
This work	Strain sensor	0-23.6%	23.6-58%	0.66	0.71
	Pressure sensor	0-4.67 kPa	4.67-12.67 kPa	0.243 kPa ⁻¹	0.041 kPa ⁻¹

Supporting Information

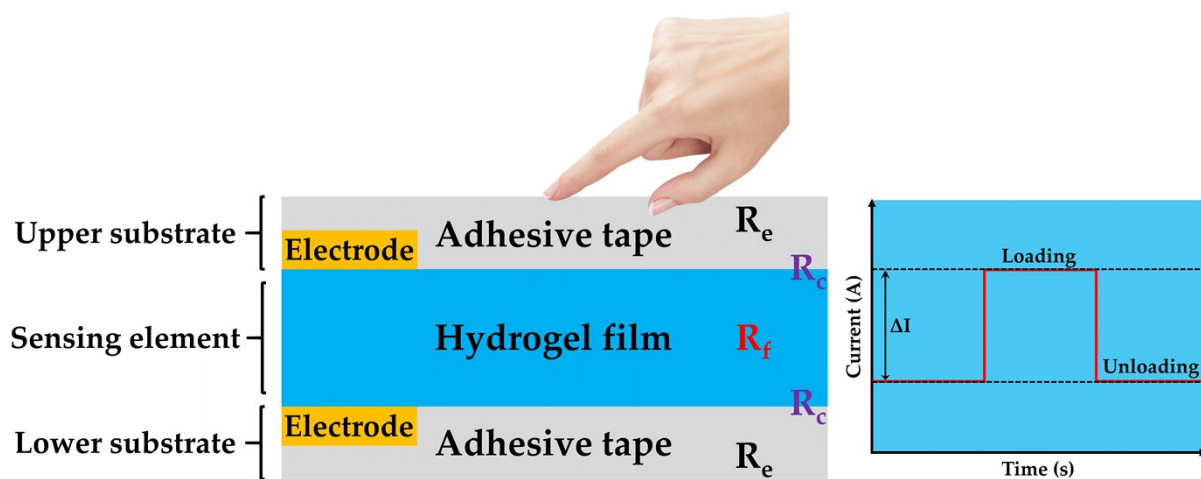


Figure S12. Device configuration of the hydrogel-based pressure sensor.

Supporting Information

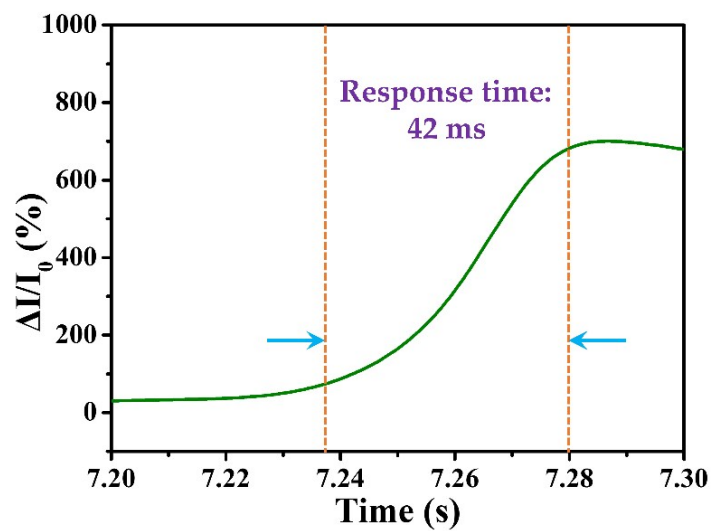


Figure S13. The response time of the hydrogel-based flexible sensor during pressure loading.

Supporting Information

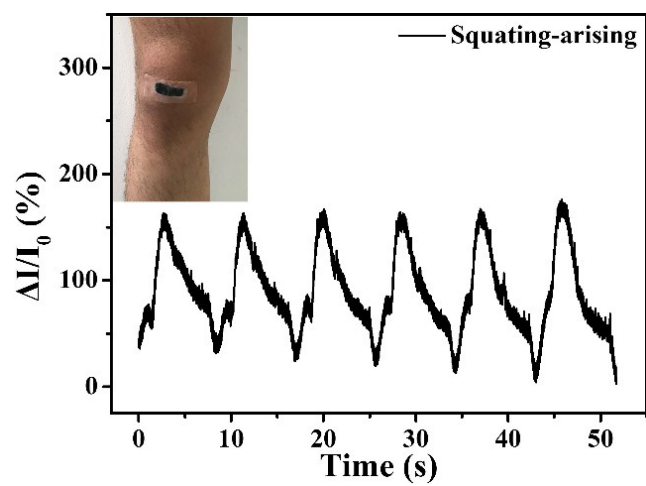


Figure S14. Current response of the sensor during the squatting-arising process.

Supporting Information

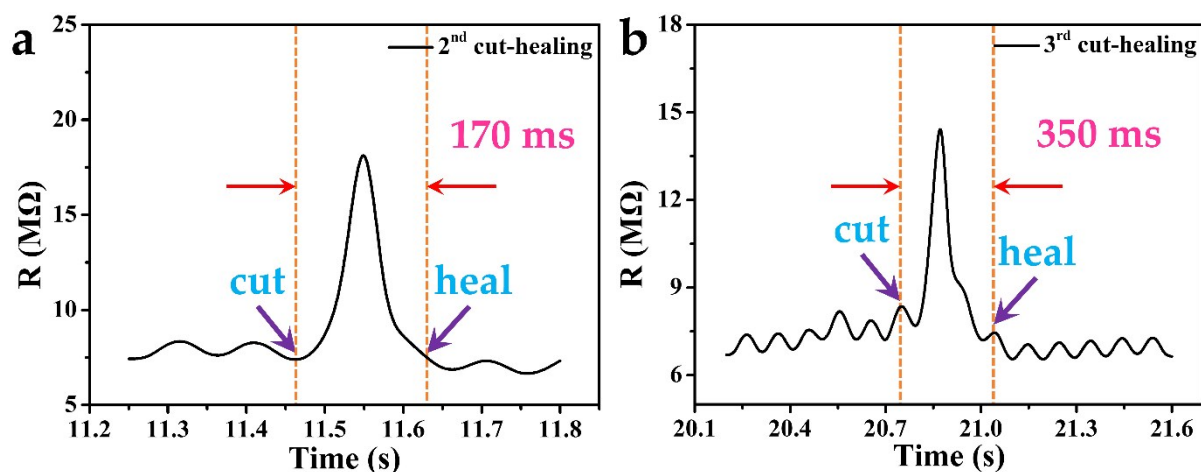


Figure S15. Electrical healing time of the hydrogel during the second and third cutting-healing process.

References

1. C. Biswas, K. K. Kim, H. Z. Geng, H. K. Park, S. C. Lim, S. J. Chae, S. M. Kim and Y. H. Lee, *J. Phys. Chem: C.*, 2009, **113**, 10044-10051.
2. Y. Zhao, J. Kang and T. Tan, *Polymer*, 2006, **47**, 7702-7710.
3. L. Pan, A. Chortos, G. Yu, Y. Wang, S. Isaacson, R. Allen, Y. Shi, R. Dauskardt and Z. Bao, *Nat. Commun.*, 2014, **5**, 3002.
4. M. Jo, K. Min, B. Roy, S. Kim, S. Lee, J. Y. Park and S. Kim, *ACS Nano*, 2018, **12**, 5637.
5. J. Liu, C. S. Y. Tan, Z. Yu, N. Li, C. Abell and O. A. Scherman, *Adv. Mater.*, 2017, **29**, 1605325.
6. H. Zhang, H. Xia and Y. Zhao, *ACS Macro. Lett.*, 2012, **1**, 1233-1236.
7. B. Liu, Y. Wang, Y. Miao, X. Zhang, Z. Fan, G. Singh, X. Zhang, K. Xu, B. Li, Z. Hu and M. Xing, *Biomaterials*, 2018, **171**, 83-96.
8. Y. Lee, S. H. Cha, Y. W. Kim, D. Choi and J. Y. Sun, *Nat. Commun.*, 2018, **9**, 1804.

Supporting Information

9. S. Liu, R. Zheng, S. Chen, Y. Wu, H. Liu, P. Wang, Z. Deng and L. Liu, *J. Mater. Chem. C.*, 2018, **6**, 4183-4190.
10. T. Li, J. Wang, L. Zhang, J. Yang, M. Yang, D. Zhu, X. Zhou, S. H.-Wang, Y. Liu and X. Zhou, *J. Mater. Chem. B.*, 2017, **5**, 5726-5732.
11. Z. Wang, H. Zhou, W. Chen, Q. Li, B. Yan, X. Jin, A. Ma, H. Liu and W. Zhao, *ACS Appl. Mater. Interfaces*, 2018, **10**, 14045-14054.
12. P. Li, Z. Jin, L. Peng, F. Zhao, D. Xiao, Y. Jin and G. Yu, *Adv. Mater.*, 2018, **30**, 1800124.
13. W. Li, F. Gao, X. Wang, N. Zhang and M. Ma, *Angew. Chem. Int. Ed.*, 2016, **128**, 9342-9347.
14. C. Xu, W. Lee, G. Dai and Y. Hong, *ACS Appl. Mater. Interfaces*, 2018, **10**, 9969-9979.
15. Z. Lei and P. Wu, *Nat. Commun.*, 2018, **9**, 1134.
16. Q. He, Y. Huang and S. Wang, *Adv. Funct. Mater.*, 2018, **28**, 1705068.
17. J. Hur, K. Im, S. W. Kim, J. Kim, D. Y. Chung, T. H. Kim, K. H. Jo, J. H. Hahn, Z. Bao, S. Hwang and N. Park, *ACS Nano*, 2014, **8**, 10066-10076.
18. S. Hong, D. Sycks, H. F. Chen, S. Lin, G. P. Loez, F. Guilak, K. W. Leong and X. Zhao, *Adv. Mater.* 2015, **27**, 4035-4040.
19. Z. Wei, J. He, T. Liang, H. Oh, J. Athas, Z. Tong, C. Wang and Z. Nie, *Polym. Chem.*, 2013, **4**, 4601-4605.
20. Y. Guo, K. Zheng and P. Wan, *Small*, 2018, **14**, 1704497.
21. K. Parida, V. Kumar, W. Jiangxin, V. Bhavanasi, R. Bendi and P. S. Lee, *Adv. Mater.*, 2017, **29**, 1702181.

Supporting Information

22. C. Shao, M. Wang, L. Meng, H. Chang, B. Wang, F. Xu, J. Yang and P. Wan, *Chem. Mater.*, 2018, **30**, 3110-3121.
23. S. H. Cho, S. W. Lee, S. Yu, H. Kim, S. Chang, D. Kang, I. Hwang, H. S. Kang, B. Jeong, Kim, H. E. S. M. Cho, K. L. Kim, H. Lee, W. Shim and C. Park, *ACS Appl. Mater. Interfaces*, 2017, **9**, 10128-10135.
24. L. Chen, J. Liu, X. Wang, B. Ji, X. Chen and B. Yang, *IEEE Trans. Electron Devices*, 2017, **64**, 1968-1972.
25. Y. Tai, M. Mülle, I. A. Ventura and G. Lubineau, *Nanoscale*, 2015, **7**, 14766-14773.
26. J. Duan, X. Liang, J. Guo, K. Zhu and L. Zhang, *Adv. Mater.*, 2016, **28**, 8037-8044.
27. Z. Lei, Q. Wang, S. Sun, W. Zhu and P. Wu, *Adv. Mater.*, 2017, **29**, 1700321.
28. G. Cai, J. Wang, K. Qian, J. Chen, S. Li and P. S. Lee, *Adv. Sci.*, 2017, **4**, 1600190.
29. Y. J. Liu, W. T. Cao, M. G. Ma and P. Wan, *ACS Appl. Mater. Interfaces*, 2017, **9**, 25559-25570.
30. Y. Tai and Z. Yang, *Adv. Mater.*, 2017, **4**, 1700496.
31. Y. Si, L. Wang, X. Wang, N. Tang, J. Yu and B. Ding, *Adv. Mater.*, 2017, **29**, 1700339.
32. Z. Lei, Q. Wang and P. Wu, *Mater. Horiz.*, 2017, **4**, 694-700.